Inkjet printability assessment of weakly viscoelastic fluid: A semi-dilute PVP solution ink case study

Pavol Suly, Jakub Sevcik, David J. Dmonte, Pavel Urbanek, Ivo Kuritka*

Centre of Polymer Systems, Tomas Bata University in Zlín, tř. Tomáše Bati 5678, 760 01 Zlín, Czech Republic

* Corresponding author: suly@utb.cz

KEYWORDS:

Polyvinylpyrrolidone, polymer solution, dimensionless criteria, viscoelasticity, inkjet printing, printability diagrams.

ABSTRACT

Here, we present an integrated approach to the weakly viscoelastic fluid printability assessment by using global dimensionless criteria (DC). The problem was studied on a model semi-diluted polyvinylpyrrolidone water-based ink. For the study purpose, the ink composition was kept as simple as possible. First, the solution density, viscosity and surface tension were determined. Obtained data was used for testing limitations of DC printability diagrams already available for Newtonian fluids. A replotted version of the original Kim & Baek's map was developed emphasising the importance of surface tension in the drop formation process. Another set of

dimensionless criteria (e.g. *Ec* and *De*) was also used for a real evaluation of the viscoelasticity effect on both jetting condition and drop formation. The polymer relaxation time as a crucial parameter for viscoelasticity was shown to be calculated using the Kuhn segment length rather than from Zimm and Rouse theories for diluted polymer systems. Then, a 2D diagram using four dimensionless criteria (*Oh* and *De* with *Ec* and *El* as parameters) is proposed based on famous McKinley's work. The diagram describes the interplay of possible forces responsible for filament thinning and break up processes. Obtained results were supported by further experiments involving drop ejection and formation, determination of critical polymer concentration and other. Proposed diagram promises a useful initial step in further investigations of viscoelasticity of polymer compounds by inkjet printing.

INTRODUCTION

Inkjet printing (IJP) represents a versatile deposition tool that reproduces digital motives on a substrate according to computer-aided pre-defined patterns or templates (from dot array up to more complex structures).[1] IJP deposition technique is based on computer-controlled ejection of fluid (called ink) drops from the print-head nozzle to a pre-specified substrate position.[2] The advantages of this deposition technique are low material consumption, low waste, no mask is needed, and it is a non-contact technique.[3] Popularity and utilisation of this technique can be demonstrated by its application fields including printed electronics (e.g. temperature[4], gas[5], and humidity[6] sensors, wearable monitoring devices[7], light-emitting diodes[8], micro-supercapacitors[9], solar cells[10,11] and others), bio-application such as a study of enzyme activity in biosensor fabrication[12], polymer artificial muscles[13], printing of collagen, fibrinogen, and thrombin[14], and printing of biological material such as cells and antibiotics[1]. Other applications include, for example, *3D* prototyping,

patterning and coating.[15–17] IJP is mostly used for the preparation of planar patterns, but three-dimensional patterns can also be prepared by layer-by-layer deposition.[18] Additionally, inkjet printing also allows controlled deposition of polymers and other functional materials.[19] Moreover, IJP enables preparation of patterns with high precision and resolution[2].

Among various methods of inkjet printing, drop on demand IJP is the most versatile and elaborate one. Inkjet printers may work in continuous or drop-on-demand (DOD) mode. The DOD method requires precise dispensing of drops of the ink. DOD mode is more suitable for preparation of patterns with precise shape because the drops are generated and deposited only when required in this mode.[2] Various approaches were established to control the printing process and develop ink formulations. Finding of the operating window in the space of process parameters for good printability is of prime interest. The term "good printability" is understood as such printing process parameters setup that ensures deposition of the ink drop to the requested place within an acceptable error and avoids unwanted defects or failures. This can be achieved by either direct single drop formation or merging of one satellite drop with the main drop during their flight usually within the travel distance less than 20 times of the characteristic length.[20] Besides numerical modelling, dimensionless criteria (DC) are considered as the most useful up to now. A list of DCs, their definition formulas, used variables, and all symbols is given in the Supporting Information SI.01. DC were successfully used for assessment of printability of Newtonian fluids based on the Weber number (*We*), the Reynolds number (*Re*), and the Ohnesorge number (*Oh*).[21] The *Z* number was implemented first based on intrinsic properties of the fluid. Fromm[22] proposed that stable drop formation was observed when $Z > 2$, Reis and Derby[23] later refined the optimum drop formation range as $10 > Z > 1$. Jang et al.[24] adjusted the printable range into the following form $14 > Z > 4$ for different fluids composition. However, the velocity of the fluid is not taken into account in the

Ohnesorge number (or in the Z number defined as $1/Oh$). Therefore, it seems necessary to consider other dimensionless numbers as well. Besides the material properties (viscosity, density, and surface tension), the tool (characteristic length), and process parameters (fluid velocity) must be taken into account. The fluid (or ink) is usually ejected through a small orifice (nozzle) at high shear rates (over 10^5 s^{-1}) and simultaneously at low values of the Reynolds number (laminar flow)[25]. This problem was successfully solved by the introduction of second DC to cover the whole triade of material-tool-process parameters, and a two-dimensional printability diagram can be obtained by plotting one DC against the other. Areas of various printability modes can be mapped in these graphs. The borderlines represent critical transition values. Such diagram was originally constructed by Derby[26] (*We* versus *Re* space) and then replotted by McKinley and Renardy[27] (*Oh* versus *Re* space). The latest most advanced diagram for Newtonian fluids was presented by Kim and Baek[20] (*Ca* versus *We* space).

Nevertheless, fluid properties depend on shear rates for non-Newtonian fluid (e.g. shear-thinning fluid). Moreover, this fluid group may show a viscoelastic character, which is typical for both polymer solutions and dispersions of nanoparticles representing the most important classes of functional inks. The influence of viscoelasticity on capillary-thinning and break-up process depends on ratios of different time-scales as the viscous time-scale, Rayleigh (or inertial) time-scale, and polymeric time-scale (polymer relaxation time). Viscoelasticity can be evaluated by another set of dimensionless criteria such as the Weissenberg number (*Wi*), the Elasticity number (*El*), the Elasto-capillary number (*Ec*), and the intrinsic Deborah number (De_0).[28] The dimensionless numbers are interrelated, and a dispensing operation can be fully described by any set of two material property based criteria and one dynamic non-dimensional groups.[29] The main problem of this approach is that it results in three-dimensional space of parameters, which is hardly

tractable for human common perception and understanding. A two-dimensional map would be highly desirable to provide simplicity and understanding, such as in the case of Newtonian fluids.

It should be pointed out, that the characteristic length obtained from the nozzle geometry corresponds precisely to the fluid filament diameter for the initial stage of the liquid ejection only. The dimensionless criteria obtained in this way are said to be "global" and are used for an overall assessment of the jet thread development dynamics. It is expected that the final outcome of the whole process depends on its initial stage and that it can be mapped in the initial values of the numbers effectively. Actually, this assumption just mirrors the requirement of the controllability of the printing process. The problem can also be treated from another point of view, and "local" critical radius of the fluid thread can be calculated under otherwise given material and processing characteristics. This is because of the characteristic length scale changes with the time of thinning.[28,29] The former approach is used in this work as we used a laboratory yet commercial printer and did not have the possibility of high accuracy time-lapse image capture and analysis where the latter approach would be more beneficial. The printability ranges based on DCs cited in this article have been developed by experiments and simulations using global criteria. Nevertheless, the potential consequences of thinning may be taken into account in cases when the global number value is close to the critical value. Finally, it must be noted that the Capillary number depends not on the characteristic length.

As has been already mentioned, IJP allows preparation of functional patterns from polymeric solutions. In this case, the polymers are dissolved in suitable solvents and together with other additives as surfactant, fillers, humectant, and colorant create a system called ink. Water-soluble polymers are one of the useful ink-forming polymers. In this case, the major part of ink formulation consists of water as a carrier medium. Polymers are usually added because of modification of the

ink properties if not being the main component. Polyvinylpyrrolidone (PVP) represents an exemplary model of a water-soluble polymer. It can be easily dissolved in cold water. PVP can be used as a capping agent to prevent the agglomeration of particles in dispersions[30], as protective compound of the perovskite grains from atmospheric moisture[31], an important part in the preparation of an *n*-type thermoelectric material based on PVP/MWCNT[32], as a noncarrier adjuvant for HIV vaccine[33], as an insulator in mixture with graphene quantum dots[34], and in many other applications[35,36]. With respect to this work, PVP has been already used in IJP applications, but mainly as rheology modifier[37], as a stabiliser in graphene ink[38], or in bio-inks to improve the viability and homogeneity of the printed cell[39]. To author's best knowledge, no article focused purely on the printability of bare PVP exist to this time, and PVP represents an ideal model for intended study.

In this work, the water solution of PVP is used as a model ink for investigation on inkjet printing of weakly viscoelastic fluids and development of their printability assessment diagram. The ink formulation was kept as simple as possible. The studied solution was chosen as the best candidate according to previous experience. The PVP was firstly dissolved in water and modified by a suitable additive, then the crucial parameters of prepared solution were determined, including solution density, viscosity and surface tension. The ink was used for the preparation of demonstrative patterns on a flexible substrate (PET film) by piezoelectric-based Dimatix material printer. Obtained data was later used for evaluation of printability of prepared polymer solution using dimensionless criteria, including the effect of viscoelasticity. First, we continued in our previous attempts to extend the use Newtonian approach[40,41], which may work for weakly viscoelastic fluids to some extent as well, especially due to emphasising of the surface tension role (Weber number). Nevertheless, the viscoelasticity must be taken into account to treat the problem

rigorously. Unlike in the Clasen work[29], a two dimensional diagram based on four dimensionless criteria (the x- and y-axis representing *Oh* and *De*, respectively, while using *Ec* and *El* as parameters) was proposed with the help of McKinley work[28] instead sectioning the three-dimensional space. A map of printability regimes was obtained. The results were supported by further experiments involving drop formation (pictures captured by integrated drop-watcher camera), determination of critical polymer concentration and other. In the last step, demonstrative pattern printed on the flexible substrate was analysed. According to our own experience, we believe that the charm of two-dimensional maps of printability is worth of attention even in the case of fluids with complex behaviour and that an easily comprehensible graphic representation of dimensionless correlations may substantially help in the process of inkjet ink development.

MATERIALS AND METHODS

Water-soluble polyvinylpyrrolidone was purchased from Sigma-Aldrich in powder form with weight-average molecular weight (M_W) around 29,000. A polyethylene glycol sorbitan monolaurate under trademark TWEEN® 20, for molecular biology grade, was used as a surfactant. Surfactant was also purchased from Sigma-Aldrich. Both compounds were used as purchased without further purification or modification. Demineralised water was used as a solvent for dissolving of PVP polymer. Polymer flexible substrate made from poly(ethylene terephthalate) (PET) NOVELE™ IJ-220 was supplied by Novacentrix (USA).

The most important parameters of each inkjet inks are viscosity, density and surface tension. Viscosity measurements of the prepared solution were carried out by using a Lovis 2000 M/ME viscometer (Anton Paar) based on the rolling ball made from steel and diameter of 1.5 mm. The measuring angle was 70°. Density measurements of solutions were performed at required

temperatures by density meter DMA5000M (Anton Paar). The surface tension (SFT) was estimated using force tensiometer K100 from KRÜSS (GmbH Germany) by plate method (also called Wilhelmy plate method). All parameters were measured in the temperature range from 25 °C to 35 °C with 5 °C increments.

The prepared polymer ink was passed through a syringe filter "LUT Syringe Filters PTFE" (Labicom s.r.o., Czech Republic) with pore size 0.24 μm to eliminate eventual insoluble particles and other impurities, and filled into cartridges (type: a piezo-driven jetting device with integrated reservoir and heater). The ink was printed by Dimatix Materials Printer DMP-2800 series (Fujifilm Dimatix, USA) onto coated PET foil. The printer head nozzles were heated to required temperature. The substrate temperature was set to 40 °C. The stand-off distance was set to 1 mm. The print-head angle was appropriately set for any needed resolution of patterns. The print-head nozzles were purged for 1 μs after every 20th run to ensure freshness of the ink.

Printed patterns were analysed by optical microscope LEICA DVM2500 Digital Camera (LEICA MICROSYSTEMS, Germany) and by optical profilometer (Bruker Corporation, USA).

RESULTS AND DISCUSSION

Preparation of polymer solution ink

The polymer solution ink was prepared by dissolving of PVP (12 wt %) in the water (87.9 wt %) at ambient temperature and continual stirring. The solution also contains the defined amount of surfactant - TWEEN® 20 (0.1 wt %). The surfactant was used for the decreasing of surface tension of water-based polymer solution ink. The 12 wt % concentration was selected as an optimum for the purpose of this study among several concentrations in a preliminary trial error test varying the

concentration from above 20 wt % (not suitable for printing at all) to 3 wt % (undesirable dripping out of the nozzle).

The intrinsic material properties

Firstly, the density and viscosity measurements were performed simultaneously. The obtained results are listed in Table 1.

Table 1. Density, dynamic viscosity, and surface tension values of prepared PVP solution determined at various temperatures. Density is expressed with six valid digits as this precision is given by the specification of the producer (Anton Paar).

Density and viscosity measurement results	Temperature 25 °C	30 °C	35 °C
Density, ρ [g/cm^3]	1.022448	1.020824	1.018993
Dynamic Viscosity [mPa s]	5.053	4.382	3.853
Kinematic Viscosity [mm²/s]	4.942	4.293	3.781
Variation Coefficient [%]	0.07	0.05	0.01
Fw/Bw Deviation [%]	0.06	0.06	0.13
Surface tension measurement results	25 °C	30 °C	35 °C
Surface tension, σ [mN/m]	35.2 ± 0.5	34.4 ± 0.5	33.2 ± 0.5

The showed data represents the average values of 10 cycles measurements with corresponding both Lovis variation coefficient (runtime repeatability in between the measurement cycles) and

Lovis Fw/Bw deviation (deviation between the runtime of a forward and the subsequent backward measurements (e.g. +70/-70° angles)[42].

As can be seen, both density and viscosity (kinematic and dynamic) of prepared ink decrease with increasing temperature. Viscosity of polymer solution can be affected by several factors, but the mostly discussed are polymer concentration, M_w of polymer and temperature. The effect of temperature was manifested by obtained results. Taking other two parameters into account, viscosity of polymer solutions increases with increasing both polymer concentration and molecular weight of polymer.[43,44] In this work, PVP with molecular weight of 29,000 was used. As mentioned, higher viscosity solution may be obtained by using the polymer with higher M_w keeping the polymer concentration same.

Although high-shear rates are expected during inkjet printing according to Wang's[25], low-shear rate viscometers and rheometers are widely used for basic characterisation of the viscosity of inkjet inks in inkjet industry as well as in academia due to their availability. This approach is justified in the literature by the evaluation of the Reynolds number related to the investigated liquid flows. The value of *Re* is very low, and the flow is in laminar regime although the shear rate is so extremely large due to the very small characteristic length.[45–47] It will be shown in a later section of this article that the prepared solution falls deeply into the laminar flow regime under the used conditions. Thus, the data obtained by used rolling-ball viscometer can be considered sufficient enough for basic characterisation of prepared inks. This data will also be used for further evaluation (printability and viscoelasticity).

It should be noted that laminar flow occurs in a pipe when the $Re \leq 2320$. Moreover, the Hagen-Poiseuille law works only for stable laminar flow, in other words, at a fully developed velocity profile. A developed velocity profile can be obtained after passing the fluid through the pipe region

called the "entrance or inlet length". The inlet length is usually defined by the Boussinesq equation as[48]:

$$x_r/A \geq 0.065 \times Re \quad (1)$$

where the x_r is the inlet length, A is the characteristic length (pipe diameter), and Re is the Reynolds number.

The measurements of surface tension (SFT or σ). were performed at the same temperature range as viscosity and density measurements. The obtained results are summarised in Table 1, as well. The surface tension was measured three times at each temperature, and the average values are reported with standard deviation. At the beginning of experiments, the SFT of water was measured for validation of used vessel and platinum Wilhelmy plate. The surface tension of water was above 72 mN/m and for 12 wt % PVP solution without surfactant around 48 mN/m at room temperature. The small addition of the surfactant (0.1 wt %) decreased the surface tension of the polymer solution to 35.2 mN/m at 25 °C. The SFT of prepared PVP solution with surfactant decreases with increasing temperature as expected.[49]

Printability prediction and evaluation using the Newtonian fluid approximation

Viscosity and SFT represent material parameters that play a key role in inkjet printing process. The viscosity is important for the performance of the ink during jetting and spreading on the substrate. The surface tension influences formation of the ink droplet as well as its spreading on the substrate. Both parameters depend on several factors, e.g. polymer concentration, ink formulation (composition), temperature and other.[50] Therefore, the producers of printing machines provide usually the simplest definition of processing (printability) window given in terms of the

suggested ranges of these two variables. As can be seen, all three parameters decrease with increasing temperature. Higher temperature may improve the jetting and drop formation.

The first and simplest approach to a weekly viscoelastic liquid may be based on treating them as Newtonian fluids and see whether such approximation gives some reliable predictions or fails. In recent years, the DCs are used for characterisation of inkjet ink. The *Z* number (defined as 1/*Oh*) is widely considered as the main criterion deciding the printability of ink. Since the *Z* number does not include any process parameter (i.e. fluid or drop velocity), other dimensionless criteria must be used for better printability evaluation. The most important criteria used for evaluation of Newtonian fluid are Reynold number (*Re*), Weber number (*We*), Ohnesorge number (*Oh*), *Z* number, and Capillary number (*Ca*). Drop velocity (6.18 m/s) of prepared PVP ink was determined by integrated drop-watcher camera (see section *The inspection of drop formation and material deposition*). The characteristic length corresponding to the hydrodynamic equivalent diameter of the printing nozzle is 21.5 μm (in the case of the used material cartridge with a nominal volume of 10 pL manufactured by Fujifilm Dimatix, Inc.[51]). The dimensionless criteria were calculated for each temperature and are shown in Table 2.

Table 2. Calculated dimensionless criteria of prepared PVP solution at different temperatures: Reynold number (*Re*), Weber number (*We*), Ohnesorge number (*Oh*), *Z* number, and Capillary number (*Ca*).

Temperature	*Re* [-]	*We* [-]	*Oh* [-]	*Z* [-]	*Ca* [-]
25 °C	26.89	23.87	0.18	5.50	0.89
30 °C	30.95	24.38	0.16	6.27	0.79
35 °C	35.14	25.23	0.14	7.00	0.72

The prepared ink should be printable judging by the value of the *Z* number solely. It falls to the printability intervals as defined by Fromm[22], Reis and Derby[23], as well as by Jang et al.[24]. To obtain a first deeper insight and include the velocity as the governing process parameter, other dimensionless criteria were considered, i.e. *Re*, *We*, *Ca*. The values of *Re* about 30 confirm the assumption of laminar flow of the ink. Moreover, development of the regular velocity profile can be expected over the inlet length about 2 times *A* which is practically negligible in comparison with the length scale of the ejected fluid filament.

Printability of PVP solution was also checked by comparison of obtained data with the general printability range area as defined by McKinley and Renardy[27], who plotted Ohnesorge number against Reynolds number. Their originally proposed diagram showing printability area ABCD was redrawn and adapted for Dimatix Materials Printer DMP-2800 using the 10 pL printing head by Maslik et al.[40] as shown in Figure 1. Here, the processing windows and operating points are calculated for the actual drop velocity of 6.18 m/s.

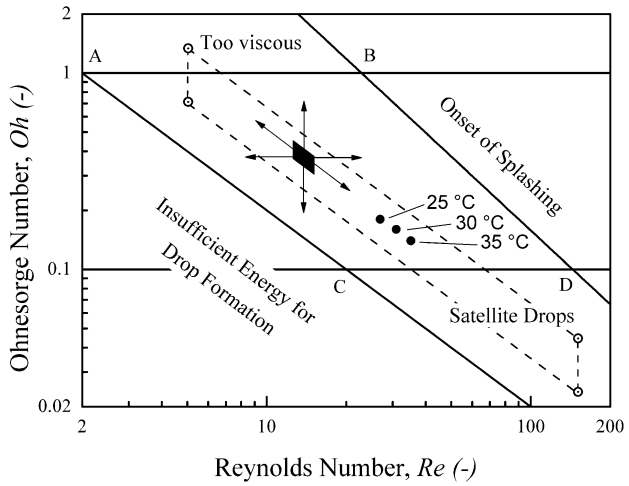

Figure 1. Replotted printability diagram with the operating space marked by ABCD showing operating space of the used printer in its suggested and maximum ranges. The solid points correspond to the tested PVP solution at various temperatures according to calculated dimensionless criteria. Adapted with permission from Ref.[40]. Copyright 2018 Sensors.

The small black full parallelogram represents the proper operational space of used Dimatix material printer considering the recommended "optimum" fluid properties (i.e., density around 1 g/cm^3, viscosity in the range of (10-12 mPa s) and SFT in the range of 28-42 mN/m).[51] Naturally, optimum fluid parameters do not have to be always fulfilled. Thus the operational space of fluids characterised by higher viscosities (up to 30 mPa s) and the surface tensions (e.g. water – 72 mN/m) declared by the printer producer[52] is drawn by open circles with central dot symbols connected by dash sides.[40] It must be noted that operational space of used material printer (small full quadrangle) was calculated with the defined characteristic length (nozzle diameter that cannot be changed for the 10 pL head) and actual drop velocity. However, the drop velocity can be controlled by process waveform. Considering all variable parameters (density, viscosity, SFT, and drop velocity), the printer process window may shift or expand or squeeze in the directions indicated by the six arrows. For a detailed description of the shifted processing window in

mentioned directions, see Maslik et al. work[40]. The position of operating points of the prepared PVP ink at different temperatures is marked by full circle data points labelled by the corresponding temperature. As can be seen, the printability of prepared polymer ink is expected. The points are aligned in line with the slope -1 which corresponds to the $We^{1/2}$ isoline at the value ca 5 because the Weber number varies with the temperature only a little. The graph can be parametrised by a set of such isolines corresponding to the following equation:

$$Oh = \sqrt{We}/Re \tag{2}$$

These hyperbolic curves are plotted as straight lines on the log-log scale. The usefulness of this approach has been already demonstrated[40,41,53]. Moreover, the obliqueness of the printability area ABCD and slope of their longer borderlines suggests the importance of the Weber number in the problem analysis. The prominent role of *We* emerging in the printability map corresponds to the importance of SFT, which is the only force responsible for the drop formation and elastic-like behaviour (retraction of the filament) in Newtonian fluids through the surface energy minimisation.[40,41,53] Actually, this was actually discerned by Derby in his pioneering work. Therefore, the obtained operating data points were also located in the printing diagram originally prepared and corrected by Derby[54]. As can be seen in Figure 2, the position of prepared ink for all three temperatures is inside of printable operational space defined by three dimensionless criteria (*Oh*, *Re*, *We*). Again, the printability of the prepared polymer ink is expected.

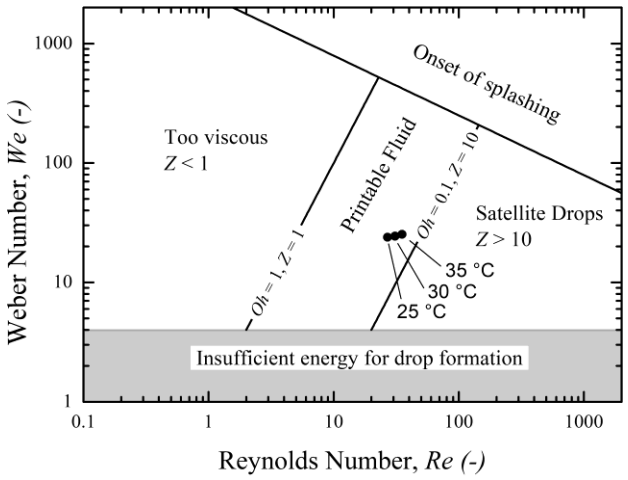

Figure 2. Printability diagram with solid points corresponding to investigated PVP solution at various temperatures according to calculated dimensionless criteria. Adapted with author`s permission from Ref.[54]. Copyright 2015 Engineering.

Additionally, both *Re* and *Ca* numbers can be used for characterisation of free surface flow of Newtonian liquids too. According to McKinley[28] and Clasen[29], these two dimensionless numbers can be plotted against each other. It is also possible to draw the original Kim and Baek's[20] map of printing regimes into a new diagram. As a result, one can obtain a generalised view of the printing process of inks.[53] The newly created diagram given by *Re vs*. *Ca* coordinates is showed in Figure 3. The prepared diagram can be used for both evaluation of the printing process of tested ink and a reconsideration of all previously defined printability limits (defined by *Z* number, for example). Moreover, this diagram merges all characteristic parameters (material, process, and tool parameters) into one graphic representation.

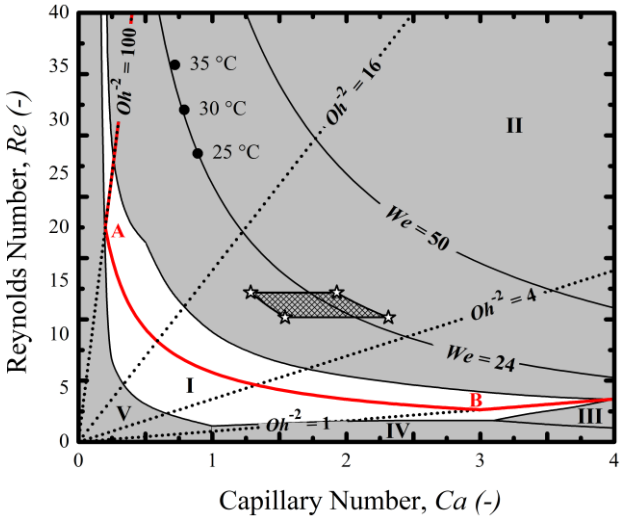

Figure 3. Printability map based on *Re*-*Ca* coordinates (Adapted with permission from Ref.[53], Copyright 2017 Tomas Bata University in Zlin).

As can be seen, the redrawn printability map can be divided into five regimes, in which different printing behaviours can be observed. Regimes are marked by Roman numerals as in the original context.[20] According to, an optimum operation window of printable fluid is represented by the white area (region I) surrounded by other regions (coloured grey). The printability regime II covers the largest part of the diagram. The transition from regime I to regime II represents a situation when the initially well-setup jetting velocity is increased beyond the printability limit and exceeds the critical value of *v* for given Oh^{-2} (inverse square of the Ohnesorge number is nothing else but the Laplace number (*La*))[53]. Other regimes are of relatively low importance in the context of this article. Thus the reader is referred to literature[20,53] for more information about the printability regimes III-V and other drawn parameters (Oh^{-2}).

Additionally (except *La*), the diagram was also enhanced by a set of contour lines along which the *We* number has a constant value. It is possible because:

$$Re = We/Ca \tag{3}$$

which gives a set of simple hyperbolic isolines. It can be seen, that points, representing the properties of prepared polymer ink at given conditions, are aligned along the contour line with *We* = 24 (as can be seen in Figure 3).

Re-inspection of *Re vs. Ca* diagram may shed light on printability evaluation. It seems that the optimum printability area has a banana-like shape. Moreover, it can be roughly delimitated by two appropriate chosen *We*-isolines. Thus, the Weber number seems to be a crucial parameter in printability evaluation. This parameter compares the effect of inertial forces to surface tension forces (see Supporting Information SI.01). In general, both viscosity and surface tension are considered as crucial parameters of inkjet inks. However, surface tension seems to be more important than viscosity in the light of new data (*We* scales with $1/\sigma$). It does not mean that the effect of viscosity is negligible and may be omitted. Moreover, the effect of η has been considered as the first and foremost important parameter of any liquid. Additionally, η represents the main parameter in all previous analyses.[53] To remind good printability can be defined as "a single drop is formed either directly without second pinch-off or the satellite drop merges with the main drop within its travel distance less than $20A$ forming thus a single drop".[20] The definition says nothing about viscosity, but it implies in its first part that there must be a mechanism causing such cohesion of the ejected liquid volume, that it forms only one drop from the beginning, which means that the mechanism causing the break up is too weak, so no break up is experienced. The latter case mentioned in the definition invokes action of a mechanism (possibly of the same cohesive physical nature), which causes acceleration of satellite drop such that it can catch up the main drop and merge with it forming one final drop.[53] Forces as the air drag and gravitation are negligible at the involved length scales and they cannot be responsible for the acceleration of the satellite drop (see Supporting Information SI.02). On the other hand, free surface of a liquid behaves like a stretched

elastic membrane. Indeed, there is the surface tension included in *We* number, which is related to the cohesion as well as break up – in other words, surface relaxation. Hence, the process is governed by the relaxation time related to surface perturbation. Next, good printability of prepared polymer ink can be achieved although the data is out of the optimum printability area (regime I) as well as the processing window of used Dimatix material printer. Therefore, the drop formation must be supported by other possible force, and the only plausible is the elastic energy.[53]

The practical importance of the diagram in Figure 3 becomes evident if we consider drop velocity as the parameter. Once we have a given ink composition, we may choose the printing head and then, the velocity remains the only parameter which can be changed freely and on-line in the printing process. Then, the graph makes the effects of the velocity change instantaneously predictable. Since Oh^{-2} involves all parameters but the velocity, the Oh^{-2} isolines visualize the trajectories that indicate relative effects of the velocity change for given ink and printing head geometry. For example, if v is doubled the distance of the corresponding point from the origin increases 2 times, and if the velocity decreases twice the operating point slides along the line towards the graph origin and its distance from the origin is halved. Similarly, the set of *We* number isolines may be used. Doubling the v increases the value of *We* by factor of 4, while halving the velocity reduces the value of *We* by factor of ¼.

The inspection of drop formation and material deposition

Deposition of the prepared PVP polymer solution was performed simultaneously with the investigation of drop ejection and formation by using available DMP 2800 Series material printer (Fujifilm Dimatix, Inc.). In this case, the cartridge with a nominal volume of drops of 10 pL was used. A jetting module of the cartridge contains 16 nozzles. Jetting (fluid ejection) is controlled by

"pulse waveform", which is a programmed voltage pulse driving a piezoelectric system. The waveform consists of several stages, and its shape is specific for each printable ink. The used waveform (consists of several stages with different parameters such as slew rate, duration a level of pulse voltage) is same for all nozzles but, drop velocity may be different at each nozzle, and it can be uniformed by jetting voltage independently at each nozzle achieving the best jetting performance. Drop formation was studied using the integrated drop-watcher camera. It allows capturing the image of drop formation at the required frequency.[51] The jetting conditions for the process of drop formation depicted in Figure 4 included a cartridge temperature of 35 °C and jetting voltage of 28 V.

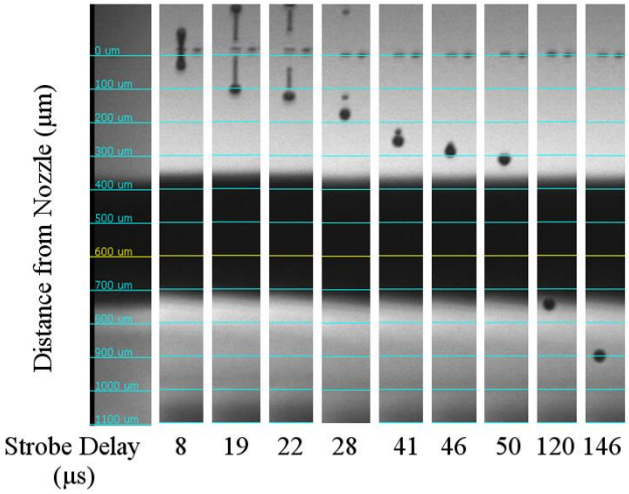

Figure 4. Ejection and drop formation of prepared polymer ink; jetting conditions were as follows: cartridge temperature of 35 °C, the voltage at the nozzle of 28 V, stand-off distance of 1mm, and cleaning cycles every 20 runs.

As can be seen in Figure 4, good printability was obtained via the merging of satellite drop with the main drop in the case of PVP solution. Based on images captured by the integrated camera, drop formation can be divided into several steps. As can be seen, the first pinch-off (detachment

of liquid thread from nozzle exit) occurred at 19 μs. Then, the ejected liquid thread is broken up (22 μs) into the main drop and liquid tail. Continuous contraction of liquid tail led to the formation of the satellite drop (around 28 μs). Later, the satellite drop caught up the main drop (first contact around 41 μs). A fully merged single drop (recombination of satellite and main drop) was observed at 50 μs in the distance over 300 μm from the nozzle. It means that only a single drop is delivered onto the required position of the substrate surface. If one takes the term of good printability into account, the satellite and main drop were recombined over the distance of 300 μm, which is in the range of 20*A* as defined by Kim and Baek[20] for the optimum printability regime.

Based on the captured images, the overall drop velocity was evaluated. Estimation of drop velocity can be found in Supporting Information SI.03.

Refinement of the analysis using viscoelasticity and printability diagram development

Viscoelasticity is an imprescriptible feature of polymeric compounds. Both viscous and elastic part must be taken into account for the complex description of polymer behaviour because already a small amount of polymer in ink may significantly affect the break-up dynamics. Addition of polymer may lead to the formation of long-lived filaments connecting the printer nozzle and ejected drops. Moreover, the length and lifetime of filaments depend on the molecular weight of the polymer as well as on the polymer concentration. If the concentration of polymer exceeds a critical value, the capillary force is not able to break the filament resulting in elastic retraction of ejected drops back to the nozzle by the filament. On the other hand, viscous liquids can be described by the Rayleigh model, which may be used with limited success for printable viscoelastic liquids as well.[55,56] It can be argued, that the Newtonian fluid formalism may be successful until

the contribution of bulk elasticity in the fluid is significantly lower than that of liquid surface elasticity.

Effect of viscoelasticity of prepared polymer solution was evaluated by a set of DC such as Weissenberg number (*Wi*), Elasticity number (*El*), Elasto-Capillary number (*Ec*), and Deborah number (*De*). In all cases, relaxation time (λ) represents a crucial parameter. However, there are several approaches to how the relaxation time can be calculated. First, relaxation time can be calculated according to Zimm and Rouse theory. Zimm relaxation time represents the longest relaxation time for a macromolecule in the polymer solution. The calculation is based on known viscosity of bare solvent and intrinsic viscosity. Rouse theory consider the similar calculation but the equation for the relaxation time contains one more constant ($6/\pi^2$) and consider a viscosity average molecular weight.[55,57] However, both approaches are valid for infinite diluted polymer solutions only (below the first critical concentration c^*). (In other words, these approaches are limited and can be useful for the printing of trace concentrations of a polymer.)

The second approach is a Kuhn segment relaxation time. In this case, the model uses the real polymer chain description (model is linked to a reptation mechanism). This model may describe the relaxation behaviour of prepared polymer solution better than first approaches (Zimm and Rouse models). Moreover, Kuhn relaxation time was also chosen with regard to the observed value of intrinsic viscosity ($c^* < c$ of the PVP solution $< c^{**}$, see Supporting Information SI.04). The relaxation time was calculated for the PVP solution at 35 °C according to the relation used by Bazilevskii et al.[58]

$$\lambda_K = \frac{2 \times \pi \times \eta \times (z_0)^3}{k_B \times T} = \frac{2 \times \pi \times (3.85 \times 10^{-3}) \times (9.62 \times 10^{-9})^3}{(1.38064852 \times 10^{-23}) \times 308.15} = \\ = 5.06 \times 10^{-6}\ s \qquad (4)$$

where $k_B \cdot T$ is the Boltzmann temperature, η is the viscosity of the solution, and the parameter z_0 defined as:

$$z_0 = b_K \times N^{\frac{1}{2}} = b_K \times \left(\frac{M_W}{\frac{b_K}{a} \times M_{mer}} \right)^{\frac{1}{2}} = (2.3 \times 10^{-9}) \times \left(\frac{29000}{14.9 \times 111} \right)^{\frac{1}{2}} = \quad (5)$$

$$= 9.62 \times 10^{-9}\, m$$

which is nothing else than real polymer chain end-to-end dimension (denoted R standardly elsewhere), where a is the monomer (actually the mer) length, b_K is the length of Kuhn segment, N is the number of Kuhn segments in macromolecule (denoted N_K standardly elsewhere), and M_{mer} is the molar mass of a monomer (mer) unit. The value of Kuhn segment length was taken from literature[59]. It should be noted, that the Kuhn relaxation time depends on Mw through viscosity and also scales with $Mw^{3/2}$ through the third power of z_0.

The filament break-up process can be controlled by three time-scales, namely Rayleigh break-up time (t_R), viscous break-up time (t_v) and polymer relaxation time. Balance between these three time-scales can be characterised by two dimensionless criteria. The first is the Ohnesorge number (ratio of viscous and Rayleigh time-scales). The second one can be expressed as "intrinsic" Deborah number (De_0) that represents the ration between polymer relaxation time and Rayleigh (or inertial) time-scale for inertia-capillary break up of an inviscid jet.[28] De_0 can be calculated according to:

$$De_0 = \frac{\lambda_K}{t_R} = \frac{\lambda_K}{\sqrt{\frac{\rho \times A^3}{\sigma}}} \quad (6)$$

In the literature[28], "intrinsic" Deborah number (De_0) is discussed for judgement of elastic forces. However, its definition (eq. 6) is considered only for inviscid jet. Considering the whole drop formation as observation time (denominator in Deborah number, see eq. 8), both Rayleigh and

viscous time scales work together as $t_R + t_v$ that may be referred as break up time.[58] From this point of view, *Ec* is also a form of the Deborah number. Then, such parameter as the "break-up-time Deborah number (De_{but})" may be adopted.

$$\frac{1}{De_{but}} = \frac{1}{De_0} + \frac{1}{Ec} = \frac{t_R}{\lambda} + \frac{t_v}{\lambda} = \frac{t_R + t_v}{\lambda} \quad (7)$$

$$De_{but} = \frac{\lambda}{t_R + t_v} \quad (8)$$

As can be seen, De_{but} consists of inverse values of De_0 number characteristic for inviscid jet and *Ec* number. If $t_R >> t_v$, the De_0 describes the situation fully. If $t_R << t_v$, the situation is governed by *Ec*. If the two relaxation times are comparable, then the break-up-time based number De_{but} might be the appropriate criterion. However, the development of this idea is at very beginning stage, and needs further investigation. Here, we stay provisionally with De_0 under softened condition of $t_R > t_v$.

Initial data were used for calculation of the second set of DC for each tested temperature. The calculated parameters are summarised in Table 3.

Table 3. Calculated dimensionless criteria of prepared PVP solution at different temperatures; Rayleigh break-up time (t_R), viscous break-up time (t_v), Relaxation time according to the Kuhn segment length (λ_K), Intrinsic Deborah number (De_0), Weissenberg number (*Wi*), Elasticity number (*El*), and Elasto-Capillary number (*Ec*). The values of the suggested break-up-time Deborah number (De_{but}) are included for illustration as well.

Temperature	t_R	t_v	λ_K	De_0	De_{but}	*Wi*	*El*	*Ec*
[°C]	[µs]	[µs]	[µs]	[-]	[-]	[-]	[-]	[-]

25	17.00	3.09	6.87	0.404	0.342	1.97	0.073	2.22
30	17.18	2.74	5.86	0.341	0.294	1.68	0.054	2.14
35	17.47	2.50	5.07	0.290	0.254	1.46	0.041	2.03

In contrast to *Wi* (see Supporting Information SI.01), both *El* and De_0 do not depend on the imposed kinematics (process parameters – velocity, *v*). The elasticity number consider only process geometry (tool, *A*) and fluid properties. The *El* number compares the effects of inertia to the effects of bulk elasticity. Obtained results correspond to processes such as spin coating or other processes for dilute polymer solution (e.g. inkjet printing) because of $El << 1$. The Elasto-Capillary number (*Ec*) allows comparing contributions of viscous and elastic effects in a (theoretically infinitely long) fluid cylinder expressing thus competition between the energy of elastic strain in the bulk and capillary forces that both work against viscous effects.[28] The bulk elastic or viscous behaviour of viscoelastic material can be evaluated according to Deborah number. If the material has a long response time relative to the observation time (a high *De*) material exhibits solid behaviour. On the other hand, the low value of *De* indicates the viscous (or fluid) behaviour.[60,61]

According to Clasen work[29], critical values of De_0 and *Ec* are 0.9766 and 4.7015, respectively. If all critical values are taken into account (including *Oh*), it is possible to create a diagram based on pioneering McKinley's work[28] that can help to decide if filament thinning is controlled by elastic, viscous or inertial forces. The prepared diagram is shown in Figure 5.

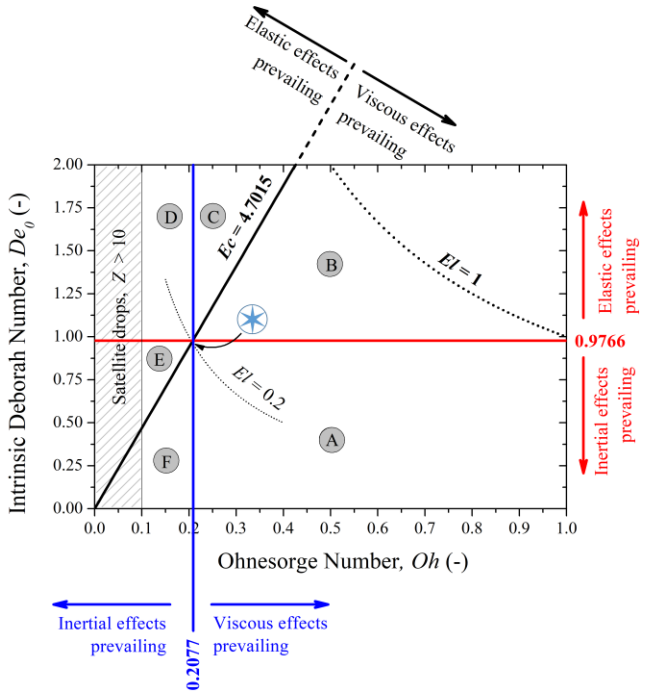

Figure 5. Proposed multifunctional diagram for evaluation of filament thinning assessment.

As can be seen, all driving forces equal at one point. This multipoint, where all areas from **A** to **F** meet, is marked by a compass rose with six cardinal directions pointing to the areas. Driving forces of every characteristic area are summarised in Supporting Information SI.05.

As can be seen, viscous effects are dominant in areas **A** and **B**. However, either inertial (area A) or elastic (area B) forces may appear here depend on the value of *De* number but they are not prevailing. Of course, area B could be divided into two subareas considering Elasticity number, but the diagram actually focusses areas below the value of $El << 1$ corresponding to processes such as spin coating, inkjet printing and other. Then, the elastic forces prevail in areas **C** and **D** with a minor effect of inertial (area D) or viscous (area C) forces. Finally, inertial forces are dominant in areas **E** and **F** below critical values of *Oh* and *De* but above the value $Oh = 0.1$, at which satellite drops are formed from ejected liquid. Here, second forces (elastic or viscous) may

assist in filament thinning depending on the degree of the elastic component in the studied system. However, It must be noted that proposed diagram (Fig. 5) describes the forces (or effects) responsible for filament thinning and break up processes considering only the material and tool properties. The process parameter (drop velocity, v) is not an explicit part of any used dimensionless number, thus, it does not describe what happens when the drop velocity is changed. If the drop velocity has to be taken into account, it should be necessary to plot *Wi vs. Oh* or *De* against *Ca*, respectively. However, we would lose some of the properties and the simplicity of borderlines between printability areas. Since *Wi* does not include t_R while *Ca* does not include characteristic length and density, which are already included in *De*, the latter option seems to be better for further investigations.

If the calculated points of prepared PVP solution will be drawn into the proposed diagram, it can be seen that all points are situated in area **F** (see Figure 6). It means that filament thinning of PVP solution is controlled predominantly by inertia with minor assists of viscous forces. Additionally, this effect becomes more dominant with increasing temperature when the operating points are shifted in direction to the graph origin (zero).

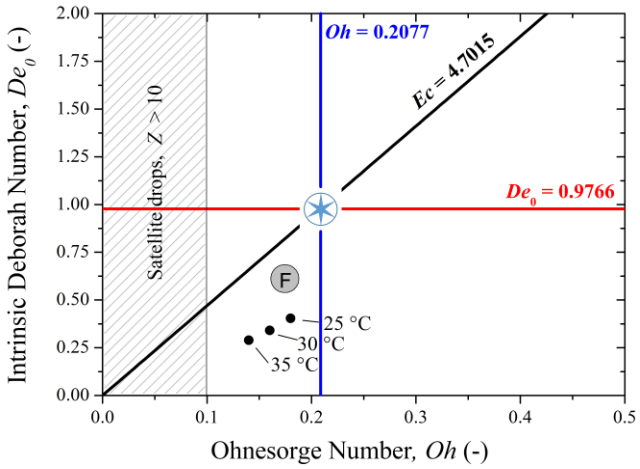

Figure 6. Position of points of prepared polymer ink in proposed multifunctional diagram for evaluation of filament thinning assessment.

Based on the obtained result, it can be concluded that filament thinning and break up processes are governed predominantly by inertia at each studied temperature. Although prepared PVP solution represents a semi-dilute solution, the polymer chain overlapping and entanglement did not occur, because the *c*** concentration limit was not exceeded. The solution operated in the hydrodynamic screening regime. It was also supported by the calculation of DCs. Based on this, no strong elastic effects was determined. The calculated values of corresponding criteria (De_0, *Wi*, *Ec*, and *El*) are smaller than their critical values representing the limit over which the elastic forces can appear. No strong elastic effects were also observed during the printing process itself. Only short filament formation (up to 100 μm, cf. *A*) was observed. As can be seen in Figure 4, the printing of PVP solution fulfilled the conditions of "good printability" although the final single drop was formed by merging of main and satellite drops.

Analysis of demonstrative patterns

Prepared ink was used for the preparation of demonstrative pre-defined patterns on modified PET substrate with surface energy of 49 mJ/m^2.[53] Surface energy was determined by sessile drop

method and evaluated according to Acid-Base theory (detailed results can be found in Supporting Information SI.06). As can be seen, a good wettability of substrate by ink was obtained. Surface energies of both ink and substrate allows to prepare a precise shape pattern without any defects. The pattern (a multi-chamber grid) was prepared with the resolution of 20 µm drop spacing (corresponding to the resolution about 1270 dpi[51]). Platen with the substrate was heated to 40 °C during printing. Prepared pattern (showed in Figure 7) was kept on the substrate holder to the next day without heating. Pattern was prepared in inert atmosphere. The prepared pattern was characterised by optical microscope and optical profilometer.

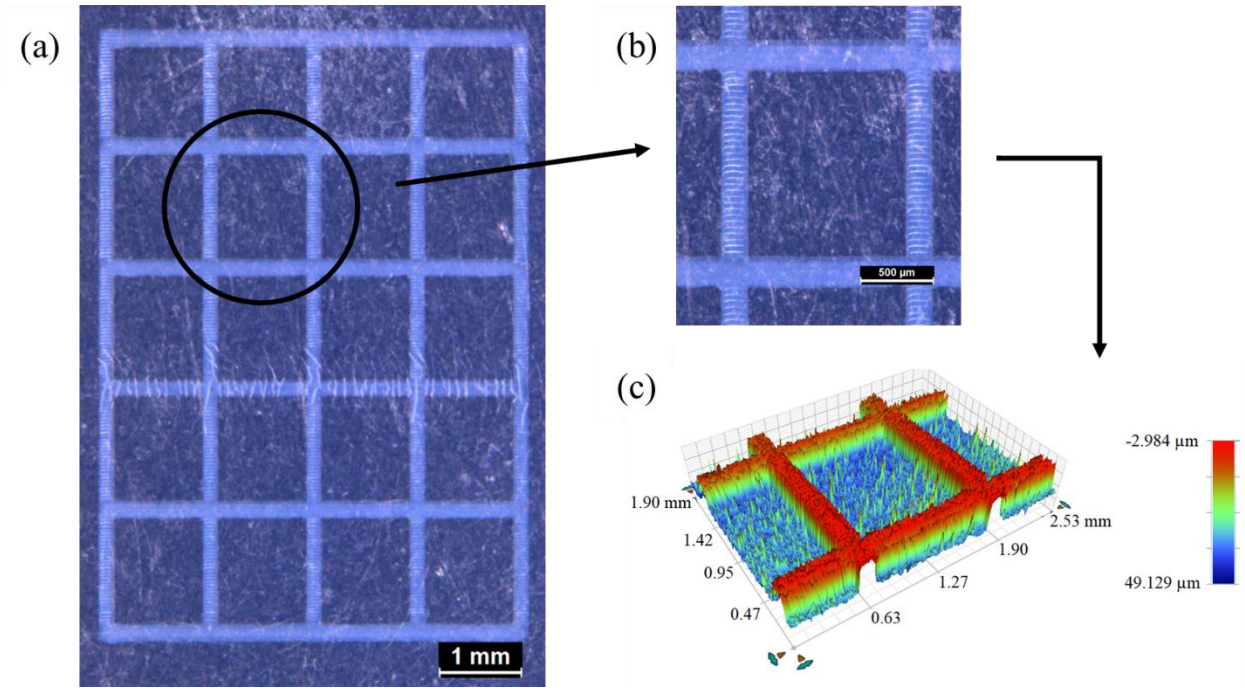

Figure 7. Full image of multi-chamber grid pattern determined by optical microscope (a) and its one box part determined by optical microscope (b) and by optical profilometer (c).

As can be seen in Figure 7, good visibility and high profile of pattern were obtained. Of course, only one box of the grid-shaped pattern was analysed due to its big size. It should be noticed that

pattern consists of one layer only. The average height of the multi-chamber grid shape pattern was about 20 μm. Images of full pattern was prepared by stitching of several images magnified 50 times.

The prepared pattern represents the most common pattern that can be used in different application ways. For example, Di Biase et al.[62] used the multi-chamber grid pattern for targeted cell seeding. Then, the open shape patterns are often prepared by different bio-inks.[63–65] On the other hand, the multi-chamber grid pattern can also be used for multi-coloured or multi-functional patterns, in which each box can be filled by different functional material. Of course, future work on prepared pattern may include, for example, water-resistance of printed PVP layers, peel-up test or above-mentioned cell tests. Moreover, polyvinylpyrrolidone can also be used for the preparation of permanent patterns because of its cross-linking possibilities.[66]

CONCLUSIONS

For printability assessment of weakly viscoelastic fluids, the polymer relaxation time plays a crucial role. However, it is necessary to choose an appropriate approach for its evaluation. In the case of semi-dilute solution, polymer relaxation time based on Kuhn segment length was found as an appropriate time scale while the other approaches (Zimm and/or Rose approaches) are not suitable because of their validity limited for highly dilute polymer solution only.

All the gathered experience together with a carefully revised state of the art theories, allowed us to propose a 2D diagram of printability assessment, which is divided into six regimes for evaluation of filament thinning and break up processes in the space between $El < 1$ and $Oh > 0.1$. The critical value 1 for El delimits solutions suitable for ink printing, spin coating etc. The Oh critical value 0.1 is a less strict limitation in this model. It might indicate multiple satellite drops formation and

thus bad printability. The printability map can help other investigators with the decision whether the filament thinning process and break up is governed by inertial, viscous or elastic forces according to critical values of *Ec* (~ 4.7), *Oh* (~ 0.2), and *De* (~ 1). In some cases, two or more of mentioned forces may show a synergic effect resulting in the formation of a single drop by merging of main and satellite drops.

For Newtonian fluids and fluids of negligible viscoelasticity, we recommend exploring our *Re vs. Ca* variant of the original Kim & Baek's map diagram, since we believe that it reflects better the nature of forces involved in the drop formation process. Moreover, it is very intuitive and can be used for immediate assessment of drop velocity changes impacts in the printing process.

This study opens a window for further investigation in different ways. In theory, the concept of break-up-time including both Rayleigh and viscous relaxation time in Deborah number might be more developed. Effects of polymer M_W on the Kuhn relaxation time can be included as well. The proposed diagram can be easily tested, verified, and adjusted if necessary in any experimental study using DOD printing of polymer solutions.

ASSOCIATED CONTENT

Supporting Information

The Supporting Information is available free of charge at:

List of dimensionless criteria with definitions and physical interpretations as well as list of characteristic time-scales with their definitions (SI.01); consideration of air drag and gravitational forces (SI.02); determination of drop velocity (SI.03); determination of an intrinsic viscosity (SI.04); table of driving forces responsible for filament thinning and break-up processes (SI.05); and determination of surface energy of used PET substrate (SI.06). (PDF)

AUTHOR INFORMATION

Corresponding Author

* **Pavol Suly** - Centre of Polymer Systems, Tomas Bata University in Zlín, tř. Tomáše Bati 5678, 760 01 Zlín, Czech Republic; https://orcid.org/0000-0002-7500-7800; Email: suly@utb.cz

Authors

Ivo Kuritka – Centre of Polymer Systems, Tomas Bata University in Zlín, tř. Tomáše Bati 5678, 760 01 Zlín, Czech Republic; https://orcid.org/0000-0002-1016-5170

Pavel Urbanek – Centre of Polymer Systems, Tomas Bata University in Zlín, tř. Tomáše Bati 5678, 760 01 Zlín, Czech Republic; https://orcid.org/0000-0002-9090-4681

Jakub Sevcik – Centre of Polymer Systems, Tomas Bata University in Zlín, tř. Tomáše Bati 5678, 760 01 Zlín, Czech Republic; https://orcid.org/0000-0003-3975-4136

David John Dmonte – Centre of Polymer Systems, Tomas Bata University in Zlín, tř. Tomáše Bati 5678, 760 01 Zlín, Czech Republic; https://orcid.org/0000-0003-4587-8071

Notes

The authors declare no competing financial interest.

ACKNOWLEDGMENT

This work was supported by the Ministry of Education, Youth and Sports of the Czech Republic – DKRVO (Number of the project: RP/CPS/2020/006).

REFERENCES

(1) Zheng, Q.; Lu, J.; Chen, H.; Huang, L.; Cai, J.; Xu, Z. Application of Inkjet Printing Technique for Biological Material Delivery and Antimicrobial Assays. *Anal. Biochem.* **2011**, *410* (2), 171–176.

(2) Li, J.; Rossignol, F.; Macdonald, J. Inkjet Printing for Biosensor Fabrication: Combining Chemistry and Technology for Advanced Manufacturing. *Lab Chip* **2015**, *15* (12), 2538–2558.

(3) Tekin, E.; Smith, P. J.; Schubert, U. S. Inkjet Printing as a Deposition and Patterning Tool for Polymers and Inorganic Particles. *Soft Matter* **2008**, *4* (4), 703–713.

(4) Vuorinen, T.; Niittynen, J.; Kankkunen, T.; Kraft, T. M.; Mäntysalo, M. Inkjet-Printed Graphene/PEDOT:PSS Temperature Sensors on a Skin-Conformable Polyurethane Substrate. *Sci. Rep.* **2016**, *6*, 35289-undefined.

(5) Yuan, Y.; Tang, X.; Jiang, L.; Yang, Y.; Zhou, Y.; Dong, Y. Convenient CNT-Paper Gas Sensors Prepared by a Household Inkjet Printer. *ACS Omega* **2020**, *5* (51), 32877–32882.

(6) Su, C. H.; Chiu, H. L.; Chen, Y. C.; Yesilmen, M.; Schulz, F.; Ketelsen, B.; Vossmeyer, T.; Liao, Y. C. Highly Responsive PEG/Gold Nanoparticle Thin-Film Humidity Sensor via Inkjet Printing Technology. *Langmuir* **2019**, *35* (9), 3256–3264.

(7) Lo, L.-W.; Zhao, J.; Wan, H.; Wang, Y.; Chakrabartty, S.; Wang, C. An Inkjet-Printed PEDOT:PSS-Based Stretchable Conductor for Wearable Health Monitoring Device Applications. *ACS Appl. Mater. Interfaces* **2021**, *13* (18), 21693–21702.

(8) Sun, W.; Xie, L.; Guo, X.; Su, W.; Zhang, Q. Photocross-Linkable Hole Transport Materials

for Inkjet-Printed High-Efficient Quantum Dot Light-Emitting Diodes. *ACS Appl. Mater. Interfaces* **2020**, *12* (52), 58369–58377.

(9) Brauniger, Y.; Lochmann, S.; Grothe, J.; Hantusch, M.; Kaskel, S. Piezoelectric Inkjet Printing of Nanoporous Carbons for Micro-Supercapacitor Devices. *ACS Appl. Energy Mater.* **2021**, *4* (2), 1560–1567.

(10) Chu, V. Ben; Siopa, D.; Debot, A.; Adeleye, D.; Sood, M.; Lomuscio, A.; Melchiorre, M.; Guillot, J.; Valle, N.; El Adib, B.; Rommelfangen, J.; Dale, P. J. Waste- And Cd-Free Inkjet-Printed Zn(O,S) Buffer for Cu(In,Ga)(S,Se)2Thin-Film Solar Cells. *ACS Appl. Mater. Interfaces* **2021**, *13* (11), 13009–13021.

(11) Meng, X.; Xu, Y.; Wang, Q.; Yang, X.; Guo, J.; Hu, X.; Tan, L.; Chen, Y. Silver Mesh Electrodes via Electroless Deposition-Coupled Inkjet-Printing Mask Technology for Flexible Polymer Solar Cells. *Langmuir* **2019**, *35* (30), 9713–9720.

(12) Bai, Y.; Zhang, D.; Guo, Q.; Xiao, J.; Zheng, M.; Yang, J. Study of the Enzyme Activity Change Due to Inkjet Printing for Biosensor Fabrication. *ACS Biomater. Sci. Eng.* **2021**, *7* (2), 787–793.

(13) Simaite, A.; Mesnilgrente, F.; Tondu, B.; Souères, P.; Bergaud, C. Towards Inkjet Printable Conducting Polymer Artificial Muscles. *Sensors Actuators, B Chem.* **2016**, *229*, 425–433.

(14) Gudapati, H.; Ozbolat, I. T. The Role of Concentration on Drop Formation and Breakup of Collagen, Fibrinogen, and Thrombin Solutions during Inkjet Bioprinting. *Langmuir* **2020**, *36* (50), 15373–15385.

(15) Singh, M.; Haverinen, H. M.; Dhagat, P.; Jabbour, G. E. Inkjet Printing-Process and Its

Applications. *Adv. Mater.* **2010**, *22* (6), 673–685.

(16) Hudd, A. Inkjet Printing Technologies. In *The Chemistry of Inkjet Inks*; Magdassi, S., Ed.; World Scientific Publishing Co. Pte. Ltd: Singapore, 2010; 3–18.

(17) Sun, J.; Li, Y.; Liu, G.; Chu, F.; Chen, C.; Zhang, Y.; Tian, H.; Song, Y. Patterning a Superhydrophobic Area on a Facile Fabricated Superhydrophilic Layer Based on an Inkjet-Printed Water-Soluble Polymer Template. *Langmuir* **2020**, *36* (33), 9952–9959.

(18) Yun, Y. H.; Kim, J. D.; Lee, B. K.; Cho, Y. W.; Lee, H. Y. Polymer Inkjet Printing: Construction of Three-Dimensional Structures at Micro-Scale by Repeated Lamination. *Macromol. Res.* **2009**, *17* (3), 197–202.

(19) De Gans, B. J.; Schubert, U. S. Inkjet Printing of Well-Defined Polymer Dots and Arrays. *Langmuir* **2004**, *20* (18), 7789–7793.

(20) Kim, E.; Baek, J. Numerical Study on the Effects of Non-Dimensional Parameters on Drop-on-Demand Droplet Formation Dynamics and Printability Range in the up-Scaled Model. *Phys. Fluids* **2012**, *24* (8), 082103.

(21) Guo, Y.; Patanwala, H. S.; Bognet, B.; Ma, A. W. K. Inkjet and Inkjet-Based 3D Printing: Connecting Fluid Properties and Printing Performance. *Rapid Prototyp. J.* **2017**, *23* (3), 562–576.

(22) Fromm, J. E. Numerical Calculation of the Fluid Dynamics of Drop-on-Demand Jets. *IBM J. Res. Dev.* **1984**, *28* (3), 322–333.

(23) Reis, N.; Derby, B. Ink Jet Deposition of Ceramic Suspensions: Modelling and Experiments of Droplet Formation. *MRS Online Proc. Libr.* **2000**, *624*, 65–70.

(24) Jang, D.; Kim, D.; Moon, J. Influence of Fluid Physical Properties on Ink-Jet Printability. *Langmuir* **2009**, *25* (5), 2629–2635.

(25) Wang, X.; Carr, W. W.; Bucknall, D. G.; Morris, J. F. High-Shear-Rate Capillary Viscometer for Inkjet Inks. *Rev. Sci. Instrum.* **2010**, *81* (6), 065106.

(26) Derby, B. Inkjet Printing of Functional and Structural Materials: Fluid Property Requirements, Feature Stability, and Resolution. *Annu. Rev. Mater. Res.* **2010**, *40*, 395–414.

(27) McKinley, G. H.; Renardy, M. Wolfgang von Ohnesorge. *Phys. Fluids* **2011**, *23* (12), 127101.

(28) Mckinley, G. Dimensionless Groups For Understanding Free Surface Flows of Complex Fluids. *Soc. Rheol. Bull.* **2005**, *74*, 6–9.

(29) Clasen, C.; Phillips, P. M.; Palangetic, L.; Vermant, and J. Dispensing of Rheologically Complex Fluids: The Map of Misery. *AIChE J.* **2012**, *58* (10), 3242–3255.

(30) Seo, K.; Sinha, K.; Novitskaya, E.; Graeve, O. A. Polyvinylpyrrolidone (PVP) Effects on Iron Oxide Nanoparticle Formation. *Mater. Lett.* **2018**, *215*, 203–206.

(31) Xiong, H.; Deluca, G.; Rui, Y.; Zhang, B.; Li, Y.; Zhang, Q.; Wang, H.; Reichmanis, E. Modifying Perovskite Films with Polyvinylpyrrolidone for Ambient-Air-Stable Highly Bendable Solar Cells. *ACS Appl. Mater. Interfaces* **2018**, *10* (41), 35385–35394.

(32) Sarabia-Riquelme, R.; Craddock, J.; Morris, E. A.; Eaton, D.; Andrews, R.; Anthony, J.; Weisenberger, M. C. Simple, Low-Cost, Water-Processable n-Type Thermoelectric Composite Films from Multiwall Carbon Nanotubes in Polyvinylpyrrolidone. *Synth. Met.*

2017, *225*, 86–92.

(33) Liu, Y.; Balachandran, Y. L.; Li, D.; Shao, Y.; Jiang, X. Polyvinylpyrrolidone-Poly(Ethylene Glycol) Modified Silver Nanorods Can Be a Safe, Noncarrier Adjuvant for HIV Vaccine. *ACS Nano* **2016**, *10* (3), 3589–3596.

(34) Ali, S.; Bae, J.; Lee, C. H.; Choi, K. H.; Doh, Y. H. All-Printed and Highly Stable Organic Resistive Switching Device Based on Graphene Quantum Dots and Polyvinylpyrrolidone Composite. *Org. Electron.* **2015**, *25*, 225–231.

(35) Teodorescu, M.; Bercea, M. Poly(Vinylpyrrolidone) – A Versatile Polymer for Biomedical and Beyond Medical Applications. *Polym. Plast. Technol. Eng.* **2015**, *54* (9), 923–943.

(36) Kobeissi, J. M.; Hassan, G. F.; Karam, P. Silver-Modified Cross-Linked Polyvinylpyrrolidone and Its Antibacterial Activity. *ACS Appl. Bio Mater.* **2018**, *1* (6), 1864–1870.

(37) Wu, S.; Zhang, Q.; Chen, Z.; Mo, L.; Shao, S.; Cui, Z. Inkjet Printing of Oxide Thin Film Transistor Arrays with Small Spacing with Polymer-Doped Metal Nitrate Aqueous Ink. *J. Mater. Chem. C* **2017**, *5* (30), 7495–7503.

(38) Santra, S.; Hu, G.; Howe, R. C. T.; De Luca, A.; Ali, S. Z.; Udrea, F.; Gardner, J. W.; Ray, S. K.; Guha, P. K.; Hasan, T. CMOS Integration of Inkjet-Printed Graphene for Humidity Sensing. *Sci. Rep.* **2015**, *5*, 17374.

(39) Ng, W. L.; Yeong, W. Y.; Naing, M. W. Polyvinylpyrrolidone-Based Bio-Ink Improves Cell Viability and Homogeneity during Drop-on-Demand Printing. *Materials (Basel).* **2017**, *10* (2), 190.

(40) Maslik, J.; Kuritka, I.; Urbanek, P.; Krcmar, P.; Suly, P.; Masar, M.; Machovsky, M. Water-Based Indium Tin Oxide Nanoparticle Ink for Printed Toluene Vapours Sensor Operating at Room Temperature. *Sensors (Switzerland)* **2018**, *18* (10), 3246.

(41) Krcmar, P.; Kuritka, I.; Maslik, J.; Urbanek, P.; Bazant, P.; Machovsky, M.; Suly, P.; Merka, P. Fully Inkjet-Printed Cuo Sensor on Flexible Polymer Substrate for Alcohol Vapours and Humidity Sensing at Room Temperature. *Sensors (Switzerland)* **2019**, *19* (14), 3068.

(42) Anton-Paar. Intrinsic Viscosity as Quality Control Parameter of PET https://www.muser-my.com/wp-content/uploads/2018/11/C72IA036EN-A.pdf (accessed May 23, 2021).

(43) Gao, C.; Xing, T.; Chen, G. Effect of Polyol Molecular Structure on Fluidity, Surface Tension, and Printed Pattern Sharpness of Disperse Dye Inks. *Langmuir* **2020**, *36* (46), 14130–14144.

(44) Peng, H.; Xie, R.; Fang, K.; Cao, C.; Qi, Y.; Ren, Y.; Chen, W. Effect of Diethylene Glycol on the Inkjet Printability of Reactive Dye Solution for Cotton Fabrics. *Langmuir* **2021**, *37* (4), 1493–1500.

(45) Pan, L.; Arratia, P. E. A High-Shear, Low Reynolds Number Microfluidic Rheometer. *Microfluid. Nanofluidics* **2013**, *14* (5), 885–894.

(46) Nie, X.; Wang, H.; Zou, J. Inkjet Printing of Silver Citrate Conductive Ink on PET Substrate. *Appl. Surf. Sci.* **2012**, *261*, 554–560.

(47) Lamont, C. A.; Eggenhuisen, T. M.; Coenen, M. J. J.; Slaats, T. W. L.; Andriessen, R.; Groen, P. Tuning the Viscosity of Halogen Free Bulk Heterojunction Inks for Inkjet Printed

Organic Solar Cells. *Org. Electron.* **2015**, *17*, 107–114.

(48) Nakayama, Y.; Boucher, R. F. Flow in Pipes. In *Introduction to Fluid Mechanics*; Butterworth-Heinemann: Oxford, 1999; 111–135.

(49) Palmer, S. J. The Effect of Temperature on Surface Tension. *Phys. Educ.* **1976**, *11* (2), 119.

(50) Magdassi, S. Ink Requirements and Formulations Guidelines. In *The Chemistry of Inkjet Inks*; Magdassi, S., Ed.; World Scientific Publishing Co. Pte. Ltd: Singapore, 2009; 19–41.

(51) FUJIFILM Dimatix, I. Dimatix Materials Printer DMP-2800 Series User Manual. *FUJIFILM Dimatix* **2010**, 1–93.

(52) FUJIFILM Dimatix, I. Jettable Fluid Formulation Guidelines https://tmi.utexas.edu/images/pdfs/fujifilm-jettable-fluid-formulation.pdf (accessed May 23, 2021).

(53) Suly, P. Study of Poly(Vinyl Alcohol) Solution for Inkjet Printing. Doctoral dissertation, Tomas Bata University in Zlín, Zlín, Czech Republic, 2017.

(54) Derby, B. Additive Manufacture of Ceramics Components by Inkjet Printing. *Engineering*. **2015**, *1* (1), 113–123.

(55) Mun, R. P.; Byars, J. A.; Boger, D. V. The Effects of Polymer Concentration and Molecular Weight on the Breakup of Laminar Capillary Jets. *J. Nonnewton. Fluid Mech.* **1998**, *74* (1–3), 285–297.

(56) De Gans, B. J.; Xue, L.; Agarwal, U. S.; Schubert, U. S. Ink-Jet Printing of Linear and Star Polymers. *Macromol. Rapid Commun.* **2005**, *26* (4), 310–314.

(57) Wheeler, J. S. R.; Yeates, S. G. Polymers in Inkjet Printing. In *Fundamentals of Inkjet Printing: The Science of Inkjet and Droplets*; Hoath, S. D., Ed.; Wiley-VCH Verlag GmbH & Co. KGaA: Weinheim, 2016; 117–140.

(58) Bazilevskii, A. V; Meyer, J. D.; Rozhkov, A. N. Dynamics and Breakup of Pulse Microjets of Polymeric Liquids. *Fluid Dyn.* **2005**, *40* (3), 376–392.

(59) Al-Saidi, W. A.; Feng, H.; Fichthorn, K. A. Adsorption of Polyvinylpyrrolidone on Ag Surfaces: Insight into a Structure-Directing Agent. *Nano Lett.* **2012**, *12* (2), 997–1001.

(60) Ebewele, R. O. Polymer Viscoelasticity. In *Polymer Science and Technology*; CRC Press LLC: Boca Raton, 2000; 382–404.

(61) Reiner, M. The Deborah Number. *Phys. Today*. **1964**, 62.

(62) Di Biase, M.; Saunders, R. E.; Tirelli, N.; Derby, B. Inkjet Printing and Cell Seeding Thermoreversible Photocurable Gel Structures. *Soft Matter* **2011**, *7* (6), 2639–2646.

(63) Kim, J. D.; Choi, J. S.; Kim, B. S.; Chan Choi, Y.; Cho, Y. W. Piezoelectric Inkjet Printing of Polymers: Stem Cell Patterning on Polymer Substrates. *Polymer (Guildf).* **2010**, *51* (10), 2147–2154.

(64) Zhuang, P.; Ng, W. L.; An, J.; Chua, C. K.; Tan, L. P. Layer-by-Layer Ultraviolet Assisted Extrusion-Based (UAE) Bioprinting of Hydrogel Constructs with High Aspect Ratio for Soft Tissue Engineering Applications. *PLoS One* **2019**, *14* (6), e0216776.

(65) Iwanaga, S.; Arai, K.; Nakamura, M. Inkjet Bioprinting. In *Essentials of 3D Biofabrication and Translation*; Atala, A., Yoo, J. J., Eds.; Academic Press is an imprint of Elsevier: London, 2015; 61–79.

(66) Anderson, C. C.; Rodriguez, F.; Thurston, D. A. Crosslinking Aqueous Poly(Vinyl Pyrrolidone) Solutions by Persulfate. *J. Appl. Polym. Sci.* **1979**, *23* (8), 2453–2462.

For Table of Contents Only.